Nucleation of vacuum bubbles in Brans-Dicke type theory

Hongsu Kim[a*], Bum-Hoon Lee[b,c†], Wonwoo Lee[c‡],
Young Jae Lee[d§] and Dong-han Yeom[d¶]

[a] *International Center for Astrophysics, KASI, Daejeon 305-348, Republic of Korea*

[b] *Department of Physics, BK21 Division, Sogang University, Seoul 121-742, Republic of Korea*

[c] *Center for Quantum Spacetime, Sogang University, Seoul 121-742, Republic of Korea*

[d] *Department of Physics, KAIST, Daejeon 305-701, Republic of Korea*

November 30, 2010

Abstract

In this paper, we study nucleation of vacuum bubbles in the Brans-Dicke type theory of gravity. In the Euclidean signatures, we calculate field combinations of vacuum bubbles as solutions of Einstein and field equations as well as their probabilities by integrating the Euclidean action. We illustrate three possible ways to obtain vacuum bubbles: true vacuum bubbles for $\omega > -3/2$, false vacuum bubbles for $\omega < -3/2$, and false vacuum bubbles for $\omega > -3/2$ when the vacuum energy of the false vacuum in the potential of the Einstein frame is *less* than that of the true vacuum. After the bubble is nucleated at the $t = 0$ surface, we can smoothly connect and match the field combinations to some solutions of the Lorentzian signatures and consistently continue their subsequent evolutions. Therefore, we conclude that, in general scalar-tensor theories or Brans-Dicke type theories, which include some models of string theory, vacuum bubbles are allowed not only in the form of true vacuum bubbles but also false vacuum bubbles, as long as a special condition is assumed on the potential.

*hongsu@kasi.re.kr
†bhl@sogang.ac.kr
‡warrior@sogang.ac.kr
§noasac@hotmail.com
¶innocent@muon.kaist.ac.kr

Contents

1 Introduction

In this paper, we study (Euclidean) vacuum bubble nucleations and their subsequent evolution dynamics in the context of the Brans-Dicke theory of gravity [1].

The Brans-Dicke theory [1] is the most studied and hence the best-known among all the alternative theories of classical gravity to Einstein's general relativity [2]. Historically, this theory has been thought of as a minimal extension of general relativity that properly accommodate both Mach's principle and Dirac's large number hypothesis [2][3]. The action of the Brans-Dicke theory takes the form

$$S_{\rm E}[g,\Phi]=\frac{1}{16\pi}\int d^4x\sqrt{-g}\left(\Phi R-\frac{\omega}{\Phi}\Phi_{;\mu}\Phi_{;\nu}g^{\mu\nu}\right), \tag{1}$$

where R is the Ricci scalar, ω is a dimensionless coupling parameter, and Φ is the Brans-Dicke field. The theory employs the viewpoint that the gravitation constant G is allowed to vary with space and time and can be written in terms of a scalar field Φ as $G=1/\Phi$. As a scalar-tensor theory of gravity, the Brans-Dicke theory involves an adjustable but undetermined Brans-Dicke parameter ω. As is well-known, the larger the value of ω, the more dominant the tensor (curvature) degree, and the smaller the value of ω, the larger the effect of the Brans-Dicke scalar. As long as we select a sufficiently large value of ω, the prediction of the theory will agree with all observations/experiments [2]. For this reason, the Brans-Dicke theory has remained a viable theory of gravity. Moreover, interesting models [4] that explain dark matter and dark energy have been developed, possibly implying that the Brans-Dicke theory may be a more relevant theory of classical gravity that is consistent with observations.

In this paper, we focus on nucleations of vacuum bubbles. It is thus convenient to use the Euclidean signatures. Generally speaking, in non-linear field theories, there are non-topological soliton configurations. These are solutions of classical field equations in pure scalar field theories with non-linear potential terms. An interesting and significant example for such a non-topological soliton configuration is the true vacuum bubble. That is, the bubble arises via quantum tunneling (i.e., the super cooled first-order cosmological phase transition) from the high temperature symmetric false vacuum state to the low temperature symmetry-breaking true vacuum state. Along this line, the dynamics of quantum tunneling was first developed by [5] in the flat space-time background and by [6] in the curved space-time background. The formulation that we shall employ in the present work can indeed be regarded as an extension or generalization of this last reference.

To study the nucleation and evolution of vacuum bubbles, we need a non-linear potential that can give different vacuum energy between each vacuum. One possible way is to include a normal scalar field with the Brans-Dicke theory. If this is possible, it will be an interesting model since

it maintains the weak equivalence principle, which was the initial motivation of the Brans-Dicke theory. However, in this paper, as a toy model and for simplicity, we introduce a potential in the Brans-Dicke field itself. In fact, if we give up the initial motivation of the Brans-Dicke theory and if we embed the theory within a more general class of theories, for example, a model of string theory or a model of scalar-tensor gravity, then such a potential and a violation of the weak equivalence principle can be a natural consequence. We call this kind of theory a Brans-Dicke *type* theory.

The Einstein equation of the Brans-Dicke type theory is determined by the potential of the Brans-Dicke field while the dynamics of the Brans-Dicke field is determined by an effective potential, which can be distinct from the original potential. Using this fact, we illustrate three possible ways to obtain vacuum bubbles: true vacuum bubbles for $\omega > -3/2$, false vacuum bubbles for $\omega < -3/2$, and false vacuum bubbles for $\omega > -3/2$ when the vacuum energy of the false vacuum in the potential of the Einstein frame is *less* than that of the true vacuum. The third solution of a false vacuum bubble is related to the authors' previous papers due to a non-minimally coupled field [7]. After the bubble is nucleated at the $t = 0$ surface, we can smoothly connect and match the field combinations to some solutions of the Lorentzian signatures and consistently continue their subsequent evolutions.

This paper is organized as follows. In Section 2, we discuss Euclidean action in Brans-Dicke type theory. In Section 3, we classify and confirm possible nucleation processes of vacuum bubbles in the Brans-Dicke type theory. In Section 4, we discuss nucleation and evolution of false vacuum bubbles in the thin wall approximation. Finally, in Section 5, we summarize and discuss related problems.

2 Euclidean action in Brans-Dicke type theory

In this section, we describe the Euclidean version of the Brans-Dicke type theory with a potential.

2.1 Brans-Dicke type theory in the Euclidean signature

The action of the Brans-Dicke type theory [1] with a potential takes the following form:

$$S_{\rm E} = \int \sqrt{g} d^4x \, \mathcal{L}_{\rm BD}, \tag{2}$$

where the Largrangian density is

$$\mathcal{L}_{\rm BD} = \frac{1}{16\pi} \left(-\Phi R + \frac{\omega}{\Phi} \Phi_{;\mu} \Phi_{;\nu} g^{\mu\nu} + V(\Phi) \right). \tag{3}$$

Here, $\sqrt{g} = \sqrt{\det g}$, Φ is the Brans-Dicke field, R is the Ricci scalar, ω is the dimensionless coupling parameter of the Brans-Dicke type theory, and $V(\Phi)$ is the potential of the Brans-Dicke field.

In this theory, the Einstein equation becomes [8]

$$G_{\mu\nu} = \frac{1}{\Phi}\left(-g_{\mu\nu}\Phi_{;\rho\sigma}g^{\rho\sigma} + \Phi_{;\mu\nu}\right) + \frac{\omega}{\Phi^2}\left(\Phi_{;\mu}\Phi_{;\nu} - \frac{1}{2}g_{\mu\nu}\Phi_{;\rho}\Phi_{;\sigma}g^{\rho\sigma}\right) - g_{\mu\nu}\frac{V(\Phi)}{2\Phi} \tag{4}$$

and the field equation of the Brans-Dicke field is

$$\Phi_{;\mu\nu}g^{\mu\nu} = \frac{1}{3+2\omega}\left(\Phi V'(\Phi) - 2V(\Phi)\right). \tag{5}$$

In the following subsections, we discuss the possible origin of our choices of the coupling ω and the potential $V(\Phi)$. In this paper, we use the convention $c = G = 1$.

2.1.1 Where does ω come from?

From observational tests, it is known that the value of ω should be greater than 4×10^4 [9]. However, in various physical models, small ω parameters can be allowed. Even though a small ω is not for our universe, if a small ω is allowed in the fundamental theory and if such a small value of ω has implications, the study of various ω will have theoretical importance.

One example is dilaton gravity, which has the effective action in the following form [10]:

$$S = \frac{1}{2\lambda_s^{d-1}}\int d^{d+1}x\sqrt{-g}e^{-\phi}\left(R + (\nabla\phi)^2\right), \tag{6}$$

where d is the space dimensions, λ_s is the length scale of string units, R is the Ricci scalar, and ϕ is the dilaton field. If we define Φ as

$$\frac{e^{-\phi}}{\lambda_s^{d-1}} = \frac{\Phi}{8\pi G_{d+1}}, \tag{7}$$

where G_{d+1} is the $d+1$ dimensional gravitation constant, then we obtain a Brans-Dicke type theory with $\omega = -1$ limit.

If there are higher loop corrections from string theory, there will be other coupling terms of ϕ. For example, the effective action from heterotic string theory compactified on a Z_N orbifold takes the following form [11]:

$$S = \frac{1}{2\lambda_s^2}\int d^4x\sqrt{-g}e^{-\phi}\left(R + (1+e^{\phi}G(\phi))(\nabla\phi)^2\right), \tag{8}$$

where

$$G(\phi) = \left(\frac{3\kappa}{2}\right)\frac{6+\kappa e^{\phi}}{(3+\kappa e^{\phi})^2} \tag{9}$$

and κ is a positive constant of order one which is determined by the coefficients of the anomaly. The coupling should then be field dependent $\omega(\Phi) = -1 - e^{\phi}G(\phi)$. In this specific model, ω depends

on λ_s and κ and it is possible to find $\omega < -1.5$. The only difference is a modification of the field equation of the Brans-Dicke field [8]:

$$\Phi_{;\mu\nu}g^{\mu\nu} = \frac{1}{3+2\omega}\left(\Phi V'(\Phi) - 2V(\Phi) - \frac{d\omega}{d\Phi}\Phi_{;\mu}\Phi_{;\nu}g^{\mu\nu}\right). \tag{10}$$

Therefore, if the variation of Φ is sufficiently small near 1, and hence the variation of $\omega(\Phi)$ is sufficiently small, a ω of less than -1.5 can be effectively justified.

In the first model of Randall and Sundrum [12], two branes are introduced to explain the hierarchy problem. Because of the warp factor between two branes, we obtain a positive tension brane and a negative tension brane in an anti de Sitter background. According to Garriga and Tanaka [13], each brane can be described by the Brans-Dicke type theory in the weak field limit with the ω parameter

$$\omega = \frac{3}{2}\left(e^{\pm s/l} - 1\right), \tag{11}$$

where s is the location of the negative tension brane along the fifth dimension, $l = \sqrt{-6/\Lambda}$ is the length scale of the anti de Sitter space, and the sign $\pm$ denotes the sign of the tension. To explain the hierarchy problem, we require $s/l \sim 35$. We then obtain a sufficiently large ω on the positive tension brane and $\omega \gtrsim -3/2$ on the negative tension brane [13][14]. However, in principle, s/l can be chosen arbitrarily, and hence one may infer that various ω near $-3/2$ may be allowed by models from brane world.

2.1.2 Effective potential: a toy model

In general, string theory predicts a non-minimal and non-universal coupling of the various fields to the dilaton [10]. Hence, it is reasonable to include the potential term in the original action, which may violate the weak equivalence principle.

For a realistic calculation, we need to choose a specific potential. In this paper, the explanation of the origin of a specific potential is not our purpose. Rather, we will choose a simple potential and observe its consequences. If the qualitative consequences do not depend on the choice of potentials, our simple toy model will maintain theoretical importance.

Note that the dependence on the potential in the field equation is complicated, and hence it is easy to fix the effective force function $F(\Phi)$ by the following form:

$$F(\Phi) \equiv \Phi V'(\Phi) - 2V(\Phi) \tag{12}$$

$$= A\left(\Phi - \Phi_{\rm t}\right)\left(\Phi - \Phi_{\rm f}\right)\left(\Phi - \left(\frac{\Phi_{\rm t} + \Phi_{\rm f}}{2} + \delta\right)\right), \tag{13}$$

where A is a positive constant, $\Phi_{\rm t}$ and $\Phi_{\rm f}$ will be the field value of the inside or outside bubble region (the subscript t denotes a true vacuum and the subscript f denotes a false vacuum), and δ

is a free parameter that determines the location of the bump of the potential. We can then choose that inside and outside regions to be in stable equilibrium in terms of the field equation.

In this paper, for convenience, we choose $\Phi_{\rm t} = 1$ and $V(\Phi_{\rm t}) = V_0$ in the true vacuum region. The potential $V(\Phi)$ and the effective potential $U(\Phi)$ then take the following form:

$$V(\Phi) = \Phi^2 \left(\int_1^\Phi \frac{F(\bar{\Phi})}{\bar{\Phi}^3} d\bar{\Phi} + V_0 \right) \tag{14}$$

and

$$U(\Phi) = \int_1^\Phi F(\bar{\Phi}) d\bar{\Phi} = \int_1^\Phi \left(\bar{\Phi} V'(\bar{\Phi}) - 2V(\bar{\Phi}) \right) d\bar{\Phi}, \tag{15}$$

where the field equation becomes $\nabla^2 \Phi = U'/(3+2\omega)$.

Note that the potential in the Einstein frame U_E is [8]

$$U_E(\Phi) = \int_1^\Phi \frac{F(\bar{\Phi})}{\bar{\Phi}^3} d\bar{\Phi} + V_0. \tag{16}$$

Of course, we have to represent U_E by a new field Φ_E, where

$$\Phi = \exp \Phi_E \sqrt{\frac{16\pi}{2\omega+3}}, \tag{17}$$

to make the canonical action in the Einstein frame. However, the relation between Φ and Φ_E is a one-to-one and onto. Therefore, the only effect is to stretch the potential along the field direction, and this does not affect the vacuum energy of each field values.

2.2 Euclidean action in Brans-Dicke type theory

Now we calculate the Euclidean action of the Brans-Dicke type theory to calculate the probability of bounces. First, we assume the $O(4)$ symmetric metric [5][6][15][16]:

$$ds_{\rm E}^2 = d\eta^2 + \rho^2(\eta)(d\chi^2 + \sin^2\chi(d\theta^2 + \sin^2\theta d\varphi^2)), \tag{18}$$

where ρ is a function that corresponds to the scale factor in the Lorentzian signature, η is the Euclidean time variable, χ, θ, and φ are angle variables of the 3-dimensional sphere.

From the metric, we find the Einstein equation for ρ and the field equation for Φ:

$$G_{\eta\eta} = 3\frac{\dot{\rho}^2 - 1}{\rho^2} = -3\frac{\dot{\rho}}{\rho}\frac{\dot{\Phi}}{\Phi} + \frac{\omega}{2}\left(\frac{\dot{\Phi}}{\Phi}\right)^2 - \frac{V}{2\Phi} \tag{19}$$

and

$$\nabla^2\Phi = \ddot{\Phi} + 3\frac{\dot{\rho}}{\rho}\dot{\Phi} \tag{20}$$

$$= \frac{1}{2\omega+3}\left(\Phi V'(\Phi) - 2V(\Phi)\right). \tag{21}$$

For convenience, we note two equivalences:

$$(\nabla\Phi)^2 = \dot{\Phi}^2, \tag{22}$$

$$\begin{aligned} \Phi R &= \omega\frac{(\nabla\Phi)^2}{\Phi} + 3\nabla^2\Phi + 2V & (23)\\ &= -\left(\frac{6}{\rho^2}\Phi\right)(\rho\ddot{\rho} + \dot{\rho}^2 - 1). & (24) \end{aligned}$$

Also, the volume factor becomes

$$\sqrt{g}d^4x = 2\pi^2\rho^3 d\eta. \tag{25}$$

Using these equations, we obtain the Euclidean action by the following:

$$\begin{aligned} S_{\rm E} &= 2\pi^2\int\rho^3 d\eta\frac{1}{16\pi}\left(-\Phi R + \omega\frac{\dot{\Phi}^2}{\Phi} + V\right) & (26)\\ &= \frac{\pi}{8}\int\rho^3 d\eta\left(\frac{6}{\rho^2}\Phi(\rho\ddot{\rho} + \dot{\rho}^2 - 1) + \omega\frac{\dot{\Phi}^2}{\Phi} + V\right). & (27) \end{aligned}$$

After integration by part, we obtain

$$S_{\rm E} = \frac{\pi}{8}\int d\eta\left(-6\dot{\Phi}\dot{\rho}\rho^2 - 6\Phi\rho\dot{\rho}^2 - 6\Phi\rho + \omega\rho^3\frac{\dot{\Phi}^2}{\Phi} + \rho^3 V\right) + \text{boundary term} \tag{28}$$

and the boundary term is negligible since we are interested in the difference between the action of an bounce and the background. Finally, after simple calculations, we obtain

$$S_{\rm E} = \frac{\pi}{4}\int d\eta\left(\rho^3 V - 6\rho\Phi\right). \tag{29}$$

This result is consistent with the result of Coleman and De Luccia [6]:

$$S_{\rm E} = 4\pi^2\int d\eta\left(\rho^3 V - \frac{3\rho}{8\pi G}\right), \tag{30}$$

and we obtain our result again if we change V by $V/16\pi$ and G by $1/\Phi$.

Finally, if we have a solution of the Euclidean metric at a stationary point, we can approximate the probability P of the Euclidean bounce by

$$P \sim Ae^{-B}, \tag{31}$$

where

$$B = S_{\rm E}(\text{bounce}) - S_{\rm E}(\text{background}). \tag{32}$$

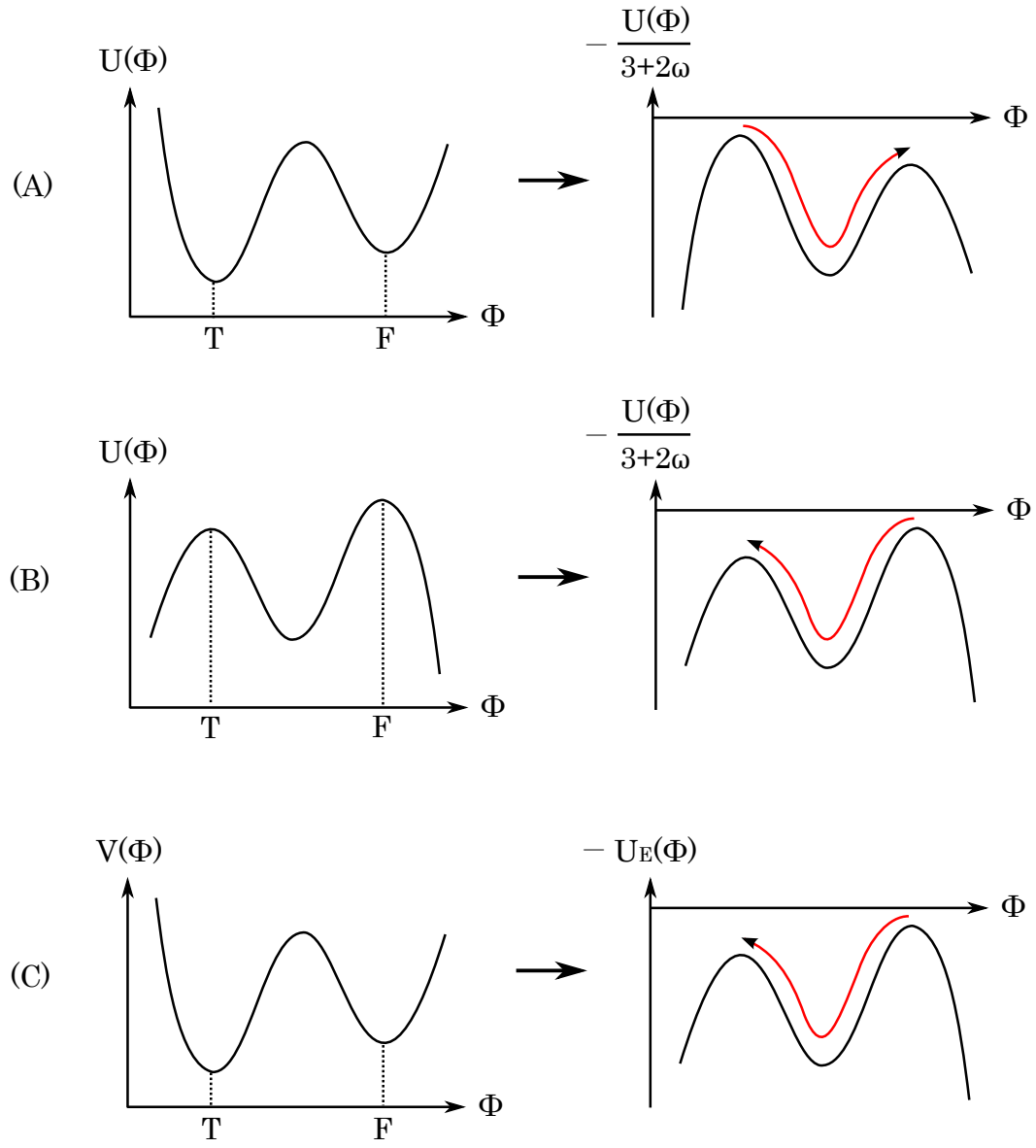

Figure 1: Possible bounce solutions in the Brans-Dicke type theory. The Lorentzian dynamics is determined by $U(\Phi)/(3+2\omega)$ while the Euclidean dynamics is determined by $-U(\Phi)/(3+2\omega)$. T and F are the location of a true vacuum and a false vacuum, respectively, in the Lorentzian signature. (A) is for $\omega > -3/2$ and means a true vacuum bubble in a false vacuum background. (B) is for $\omega < -3/2$ and means a false vacuum bubble in a true vacuum background. (C) is for $\omega > -3/2$, where $V(T) < V(F)$ and $U_E(T) > U_E(F)$; hence a nucleation of a false vacuum bubble is possible.

background	bubble	A	δ	V_0	$\Phi_{\rm f}-\Phi_{\rm t}$
dS	dS	10^4	$\mp\,0.0025$	$\mathfrak{V}$	$\mp\,0.025$
dS	Flat	10^4	$\mp\,0.0025$	0	$\mp\,0.025$
dS	AdS	10^4	$\mp\,0.0025$	$-\mathfrak{V}$	$\mp\,0.025$
Flat	AdS	10^4	$\mp\,0.0025$	$-2\mathfrak{V}$	$\mp\,0.025$
AdS	AdS	10^4	$\mp\,0.0025$	$-3\mathfrak{V}$	$\mp\,0.025$

Table 1: Potentials $V(\Phi)$ for true vacuum bubble bounces. The upper signs of $\pm$ are for $\Phi_{\rm f}<1$ (Figure 2) and the lower signs of $\pm$ are for $\Phi_{\rm f}>1$ (Figure 3). Here, $\mathfrak{V}=3.092\times10^{-5}$ for $\Phi_{\rm f}<1$ and $\mathfrak{V}=3.418\times10^{-5}$ for $\Phi_{\rm f}>1$.

3 Nucleation of vacuum bubbles in Brans-Dicke type theory

In this section, we illustrate and confirm possible bounce solutions of the Brans-Dicke type theory. The dynamics of the field is determined by the field equation

$$\ddot{\Phi}+3\frac{\dot{\rho}}{\rho}\dot{\Phi}=\frac{1}{2\omega+3}\frac{dU}{d\Phi}=-\frac{d}{d\Phi}\frac{-U}{2\omega+3}, \tag{33}$$

and hence it is determined by $-U(\Phi)/(3+2\omega)$. The second term of the left hand side is the damping term and it is reasonable to infer that the field will tend to stop to roll in most situations. However, the energy-momentum tensor is given by $V(\Phi)$, and hence the meaning of a false or true vacuum is determined by $V(\Phi)$.

In Figure 1, we classify possible bounce solutions. The left diagrams of Figure 1 are typical effective potentials $U(\Phi)$ or potentials $V(\Phi)$. Let us first consider the cases $V(T)<V(F)$ and $U(T)<U(F)$, where T is the field value of the true vacuum and F is the field value of the false vacuum. (A) in Figure 1 is for $\omega>-3/2$ and describes the generation of a true vacuum bubble in a false vacuum background. (B) is for $\omega<-3/2$ and describes a false vacuum bubble in a true vacuum background. However, if $V(T)<V(F)$ and $U(T)>U(F)$, then there may be a false vacuum bubble even in the $\omega>-3/2$ case. Note that the sufficient condition is not only $U(T)>U(F)$ but also $U_E(T)>U_E(F)$ (this will be confirmed in the following subsections). (C) is a situation for $\omega>-3/2$, where $V(T)<V(F)$ and $U_E(T)>U_E(F)$; hence a nucleation of a false vacuum bubble is possible.

In the following subsections, we numerically confirm the possibilities of the bounce solutions in detail.

background	bubble	A	δ	V_0	$\Phi_{\rm f} - \Phi_{\rm t}$
dS	dS	-10^4	$\pm$ 0.0025	$\mathfrak{V}$	$\mp$ 0.025
Flat	dS	-10^4	$\pm$ 0.0025	0	$\mp$ 0.025
AdS	dS	-10^4	$\pm$ 0.0025	$-\mathfrak{V}$	$\mp$ 0.025
AdS	Flat	-10^4	$\pm$ 0.0025	$-2\mathfrak{V}$	$\mp$ 0.025
AdS	AdS	-10^4	$\pm$ 0.0025	$-3\mathfrak{V}$	$\mp$ 0.025

Table 2: Potentials $V(\Phi)$ for false vacuum bubble bounces. The upper signs of $\pm$ or $\mp$ are for $\Phi_{\rm f} < 1$ (Figure 6) and the lower signs of $\pm$ or $\mp$ are for $\Phi_{\rm f} > 1$ (Figure 7). Here, $\mathfrak{V} = 3.336 \times 10^{-5}$ for $\Phi_{\rm f} < 1$ and $\mathfrak{V} = 3.174 \times 10^{-5}$ for $\Phi_{\rm f} > 1$.

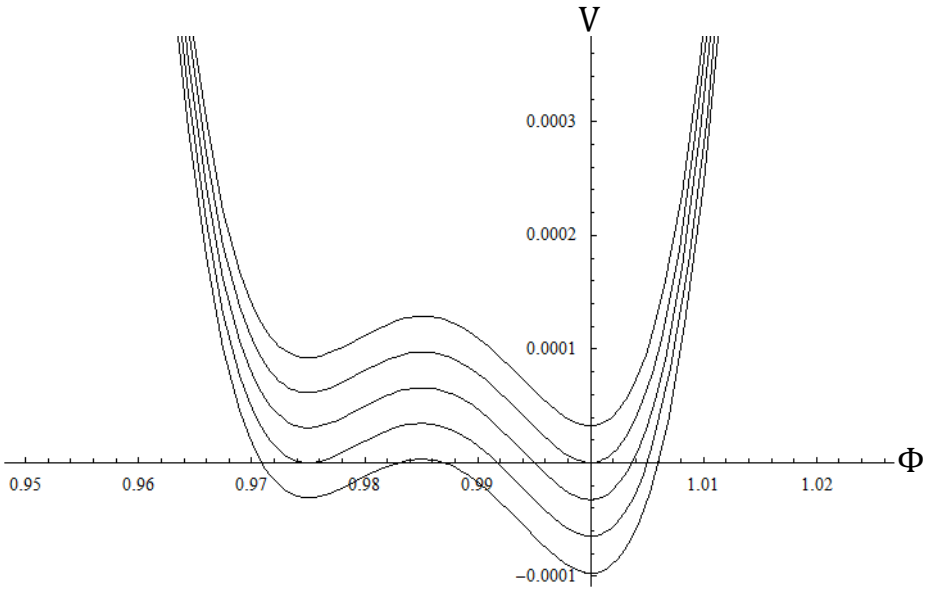

Figure 2: Potentials $V(\Phi)$ for $A = 10^4$, $\delta = -0.0025$, $\Phi_{\rm f} - \Phi_{\rm t} = -0.025$, and hence for $\Phi_{\rm f} < 1$. We choose V_0 as in Table 1 to vary the true vacuum energy. From top to bottom, each potential describes a de Sitter background and a de Sitter bubble, a de Sitter background and a flat bubble, a de Sitter background and an anti de Sitter bubble, a flat background and an anti de Sitter bubble, and an anti de Sitter background and an anti de Sitter bubble.

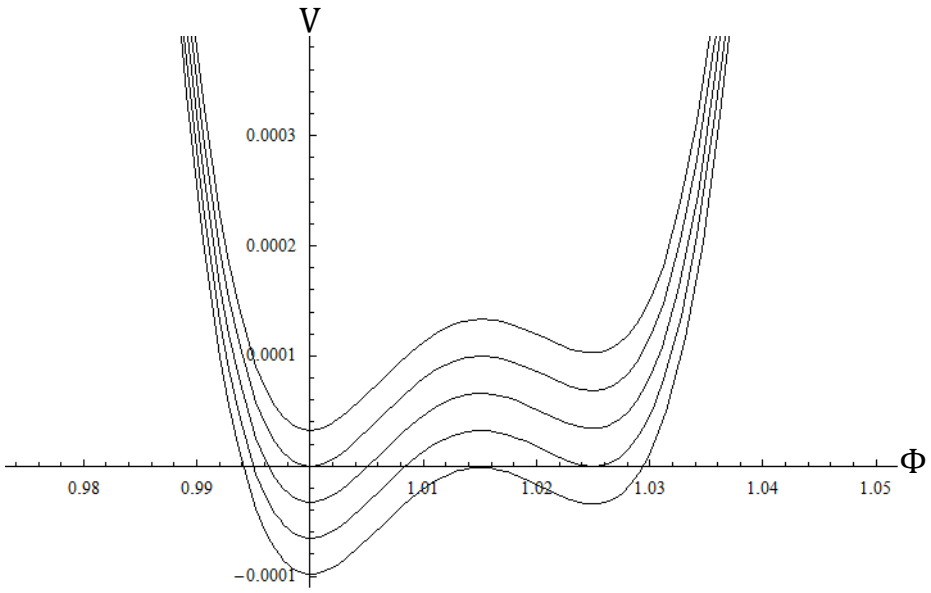

Figure 3: Potentials $V(\Phi)$ for $A = 10^4$, $\delta = 0.0025$, $\Phi_{\rm f} - \Phi_{\rm t} = 0.025$, and hence for $\Phi_{\rm f} > 1$. We choose V_0 as in Table 1 to vary the true vacuum energy.

3.1 $\omega > -3/2$: true vacuum bubbles in false vacuum backgrounds

First, we consider true vacuum bubbles in false vacuum backgrounds. There are 5 possibilities: a de Sitter bubble in a de Sitter background, a flat bubble in a de Sitter background, an anti de Sitter bubble in a de Sitter background, an anti de Sitter bubble in a flat background, and an anti de Sitter bubble in an anti de Sitter background. Also there are two possibilities for $\Phi_{\rm f}$, depending on whether it is more or less than 1. Therefore, to study these possibilities, we considered 10 potentials, as illustrated in Table 1. Here, we used $\omega = 10$, and hence it is greater than $-3/2$. Figures 2 and 3 show the potentials we used.

3.1.1 $\Phi_{\rm f} < 1$

In Figure 4, we denote bounce solutions for true vacuum bubbles in false vacuum backgrounds by potentials in Figure 2 ($\Phi_{\rm f} < 1$). We plot Φ, ρ, and $\dot{\rho}$ as functions of η.

3.1.2 $\Phi_{\rm f} > 1$

In Figure 5, we denote bounce solutions for true vacuum bubbles in false vacuum backgrounds by potentials in Figure 3 ($\Phi_{\rm f} > 1$). We plot Φ, ρ, and $\dot{\rho}$ as functions of η.

Note that ρ is a sin function for a de Sitter space, proportional to η for a flat space, and a sinh function for an anti de Sitter space. Therefore, $\dot{\rho}$ is a cos function for a de Sitter space, 1 for a flat

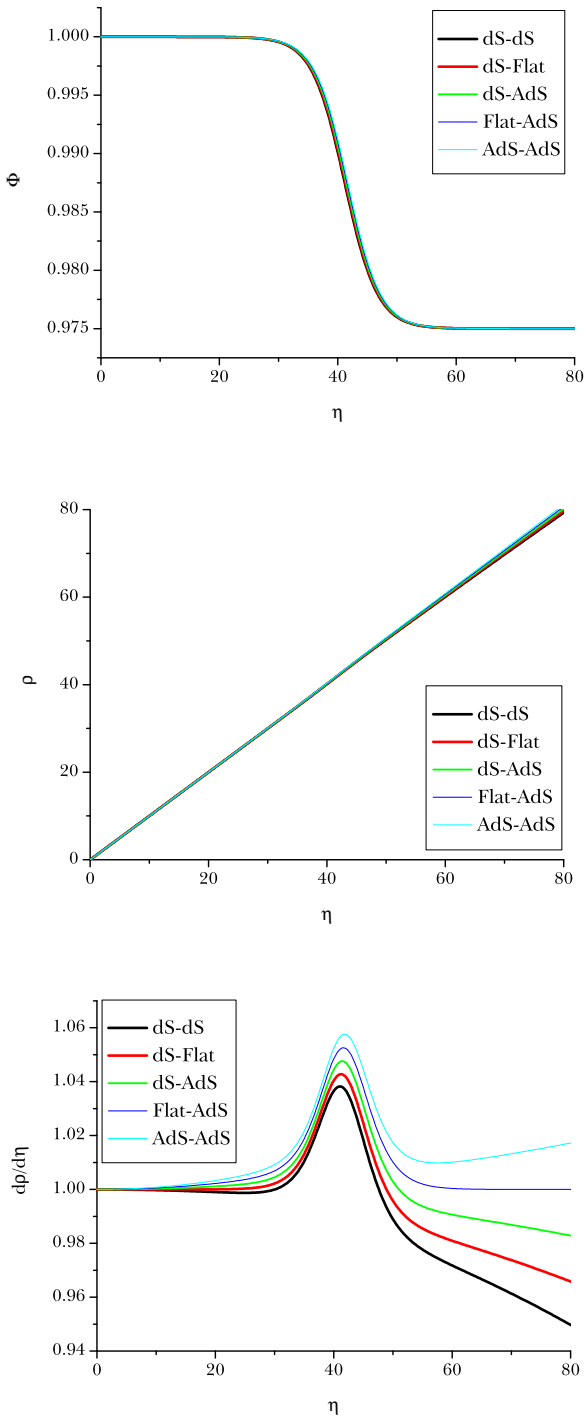

Figure 4: For $\omega > -3/2$, we illustrate bounce solutions for true vacuum bubbles in false vacuum backgrounds by potentials in Figure 2 ($\Phi_{\rm f} < 1$). Initial conditions are in Table 4 ($\delta < 0$ and $\Phi_{\rm f} - \Phi_{\rm t} < 0$). We plot Φ, ρ, and $\dot{\rho}$ as functions of η. Each caption for each curve describes a background and a bubble (e.g., dS $-$ dS describes a de Sitter background and a de Sitter bubble).

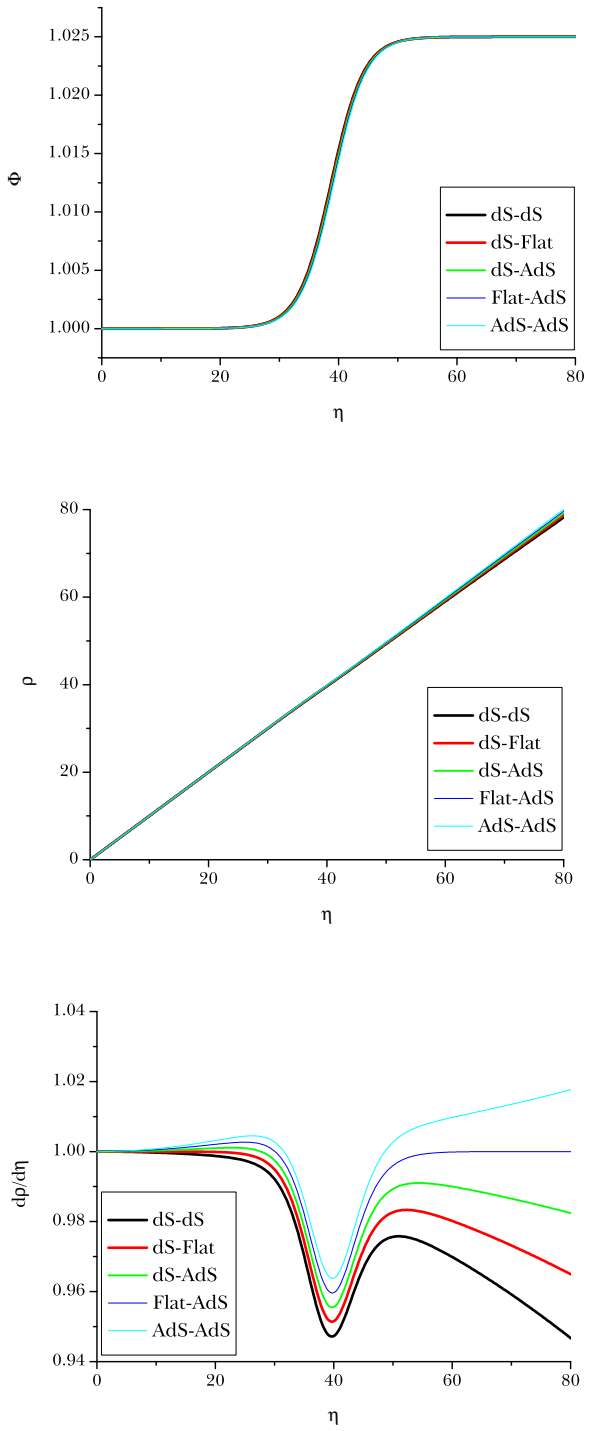

Figure 5: For $\omega > -3/2$, we illustrate bounce solutions for true vacuum bubbles in false vacuum backgrounds by potentials in Figure 2 ($\Phi_{\rm f} < 1$). Initial conditions are in Table 4 ($\delta > 0$ and $\Phi_{\rm f} - \Phi_{\rm t} > 0$). We plot Φ, ρ, and $\dot{\rho}$ as functions of η. Each caption for each curve describes a background and a bubble (e.g., dS $-$ dS describes a de Sitter background and a de Sitter bubble).

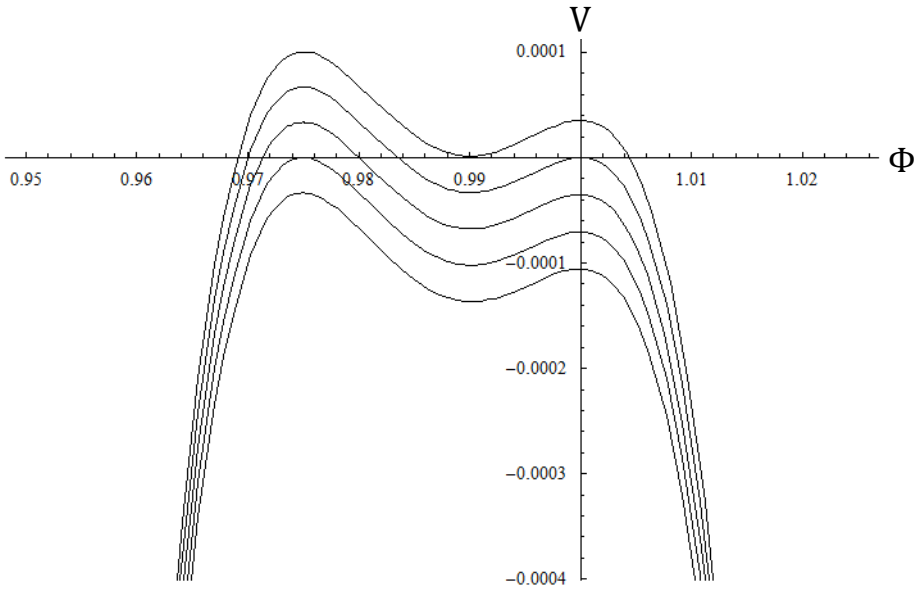

Figure 6: Potentials $V(\Phi)$ for $A = -10^4$, $\delta = 0.0025$, $\Phi_{\rm f} - \Phi_{\rm t} = -0.025$, and hence for $\Phi_{\rm f} < 1$. We choose V_0 as in Table 2 to vary the true vacuum energy. From top to bottom, each potential means a de Sitter background and a de Sitter bubble, a flat background and a de Sitter bubble, an anti de Sitter background and a de Sitter bubble, an anti de Sitter background and a flat bubble, and an anti de Sitter background and an anti de Sitter bubble.

space, and a cosh function for an anti de Sitter space. In our results, ρ is too close to compare, but $\dot{\rho}$ can be distinguishable. Such behaviors (cos, 1, cosh, etc.) consistently hold for the inside and the outside of the transition region.

3.2 $\omega < -3/2$: false vacuum bubbles in true vacuum backgrounds

Second, we consider false vacuum bubbles in true vacuum backgrounds. There are 5 possibilities: a de Sitter bubble in a de Sitter background, a de Sitter bubble in a flat background, a de Sitter bubble in an anti de Sitter background, a flat bubble in an anti de Sitter background, and an anti de Sitter bubble in an anti de Sitter background. Also, there are two possibilities for $\Phi_{\rm f}$, depending on whether it is more or less than 1. Therefore, to study these possibilities, we considered 10 potentials, as illustrated in Table 2. Here, we used $\omega = -2$, and hence it is less than $-3/2$. Figures 6 and 7 show the potentials we used.

It should be noted that two peaks in potentials Figures 6 and 7 are *stable* vacua for $\omega < -3/2$. This is obvious since the dynamics of the field is determined by the field equation in the Lorentzian

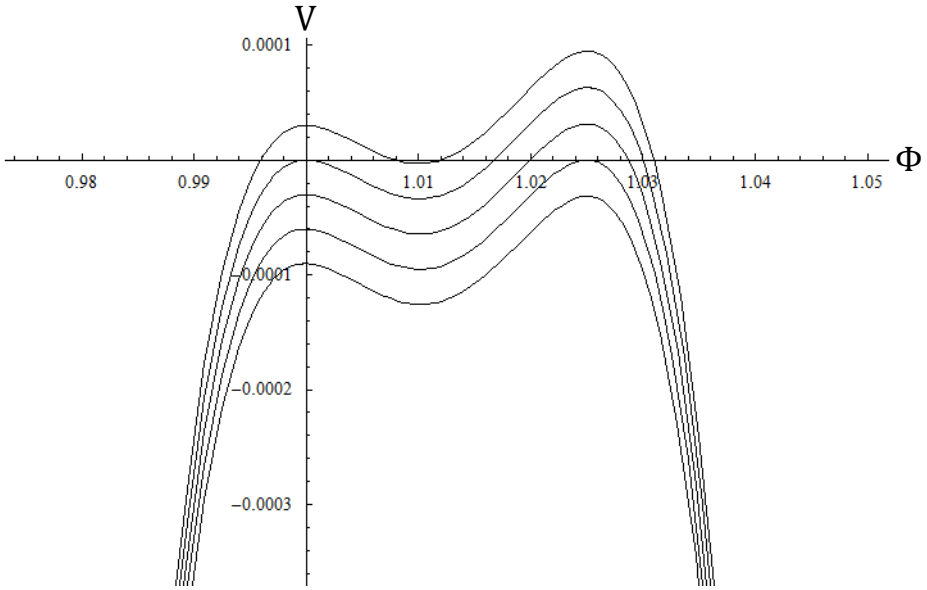

Figure 7: Potentials $V(\Phi)$ for $A = -10^4$, $\delta = -0.0025$, $\Phi_{\rm f} - \Phi_{\rm t} = 0.025$, and hence for $\Phi_{\rm f} > 1$. We choose V_0 as in Table 2 to vary the true vacuum energy.

signatures

$$\ddot{\Phi} + 3\frac{\dot{\rho}}{\rho}\dot{\Phi} = -\frac{1}{2\omega+3}\frac{dU}{d\Phi} = \frac{1}{|2\omega+3|}\frac{dU}{d\Phi}, \tag{34}$$

and hence it is determined by $-U(\Phi)/|2\omega+3|$.

3.2.1 $\Phi_{\rm f} < 1$

In Figure 8, we denote bounce solutions for false vacuum bubbles in true vacuum backgrounds by potentials in Figure 6 ($\Phi_{\rm f} < 1$). We plot Φ, ρ, and $\dot{\rho}$ as functions of η.

3.2.2 $\Phi_{\rm f} > 1$

In Figure 9, we denote bounce solutions for false vacuum bubbles in true vacuum backgrounds by potentials in Figure 7 ($\Phi_{\rm f} > 1$). We plot Φ, ρ, and $\dot{\rho}$ as functions of η.

We also note that behaviors of $\dot{\rho}$ (cos, 1, cosh, etc.) are consistent for the inside and the outside of the transition region.

3.3 False vacuum bubble nucleation via effective potentials

Although $V(\Phi_{\rm t}) < V(\Phi_{\rm f})$, if the vacuum energy of $\Phi_{\rm f}$ in the Einstein frame is smaller than that of $\Phi_{\rm t}$, i.e., $U_E(\Phi_{\rm t}) > U_E(\Phi_{\rm f})$ where U_E is the potential of the Einstein frame, it may be possible

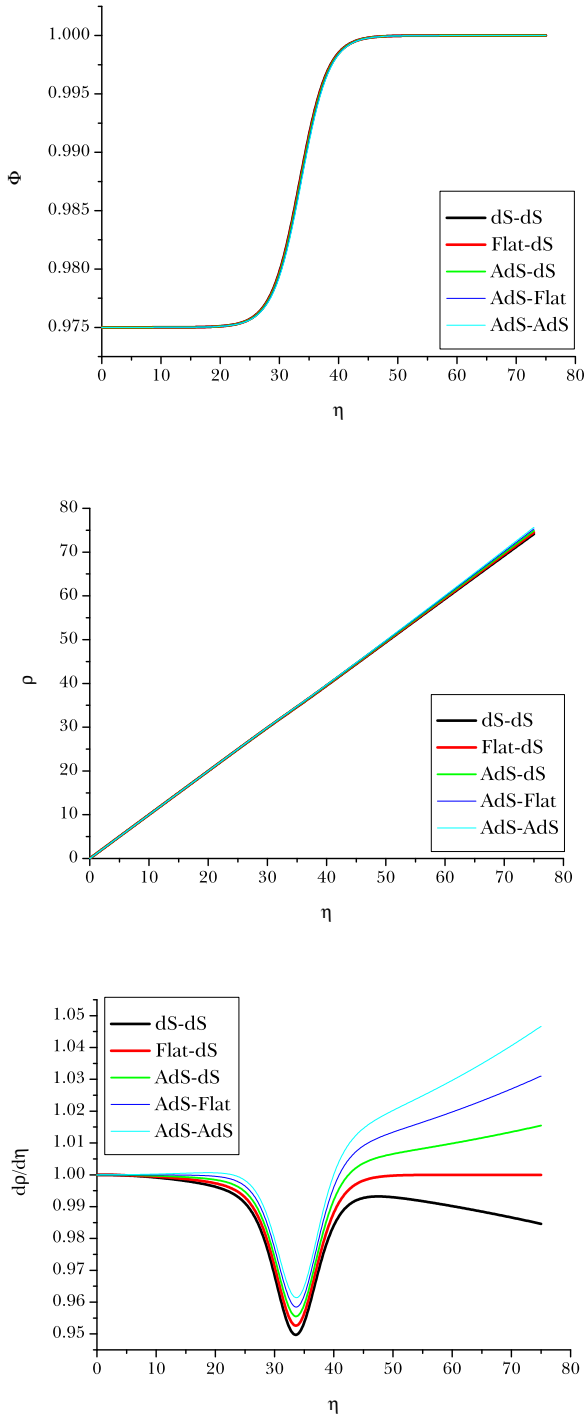

Figure 8: For $\omega < -3/2$, we illustrate bounce solutions for false vacuum bubbles in true vacuum backgrounds by potentials in Figure 6 ($\Phi_{\rm f} < 1$). Initial conditions are in Table 4 ($\delta > 0$ and $\Phi_{\rm f} - \Phi_{\rm t} < 0$). We plot Φ, ρ, and $\dot{\rho}$ as functions of η. Each caption for each curve means a background and a bubble (e.g., dS $-$ dS means a de Sitter background and a de Sitter bubble).

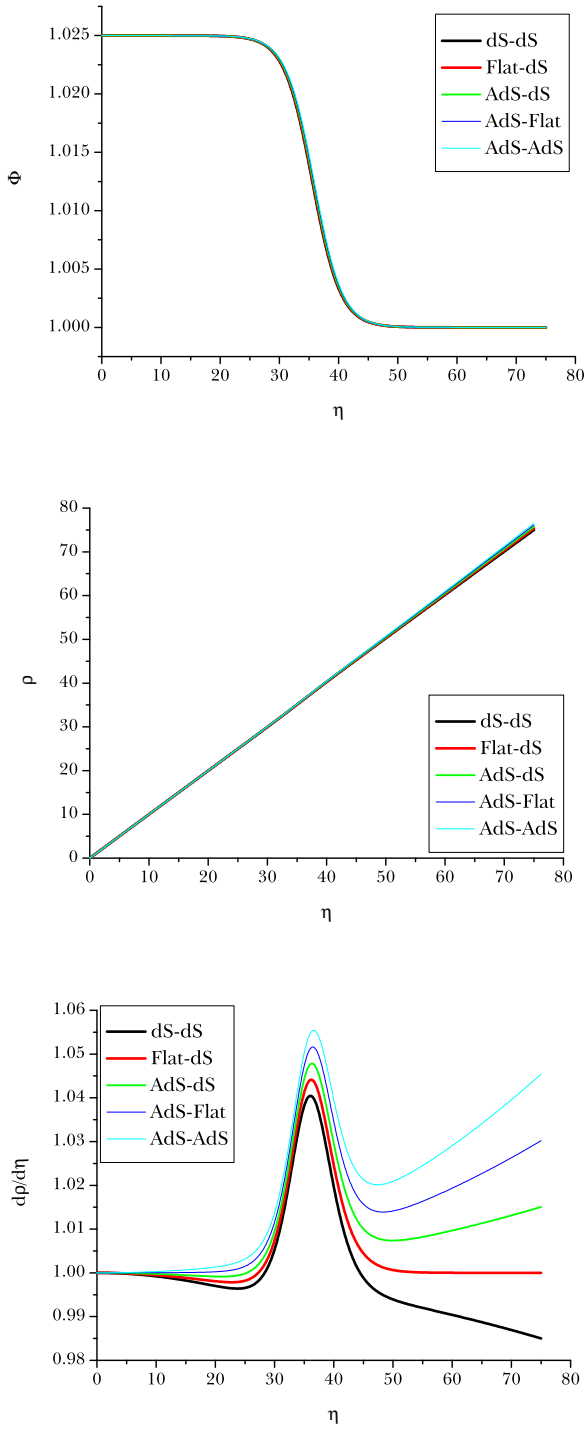

Figure 9: For $\omega < -3/2$, we illustrate bounce solutions for false vacuum bubbles in true vacuum backgrounds by potentials in Figure 7 ($\Phi_{\rm f} > 1$). Initial conditions are in Table 4 ($\delta < 0$ and $\Phi_{\rm f} - \Phi_{\rm t} > 0$). We plot Φ, ρ, and $\dot{\rho}$ as functions of η. Each caption for each curve means a background and a bubble (e.g., dS − dS means a de Sitter background and a de Sitter bubble).

to obtain a false vacuum bubble in the Jordan frame, even if $\omega > -3/2$. Note that the dynamics of the Brans-Dicke field is determined by the effective potential U. Hence, we also must find $U(\Phi_{\rm t}) > U(\Phi_{\rm f})$.

Such conditions can be represented as:

$$V(\Phi_{\rm f}) - V(\Phi_{\rm t}) = \Phi_{\rm f}^2 \left(\int_1^{\Phi_{\rm f}} \frac{F(\bar{\Phi})}{\bar{\Phi}^3} d\bar{\Phi} + V_0 \right) - V_0 > 0 \tag{35}$$

and

$$U_E(\Phi_{\rm f}) - U_E(\Phi_{\rm t}) = \int_1^{\Phi_{\rm f}} \frac{F(\bar{\Phi})}{\bar{\Phi}^3} d\bar{\Phi} \equiv \Delta E < 0. \tag{36}$$

Therefore, we require $V_0 > \Phi_{\rm f}^2 |\Delta E|/(\Phi_{\rm f}^2 - 1)$ and we conclude that such false vacuum bubbles can be possible only in a de Sitter space background ($V_0 > 0$) if $\Phi_{\rm f} > 1$. (In the next section, we discuss that a false vacuum bubble can expand in the Lorentzian signatures only if $\Phi_{\rm f} > 1$. Hence, we only consider this case.)

If we choose parameters $\omega = 10$, $A = 10^4$, $\Phi_{\rm f} - \Phi_{\rm t} = 0.01$, $\delta = -0.001$, and $V_0 = 0.0001$, we obtain potentials for such conditions (Figure 10). Here, we denote V, U_E, and U. We find that $V(\Phi_{\rm t}) < V(\Phi_{\rm f})$, and hence $\Phi_{\rm f}$ is in a false vacuum in the Jordan frame, but $U_E(\Phi_{\rm t}) > U_E(\Phi_{\rm f})$ and $U(\Phi_{\rm t}) > U(\Phi_{\rm f})$. Therefore, $\Phi_{\rm f}$ is in a true vacuum in the Einstein frame. If a true vacuum bubble can be generated in the Einstein frame [6], it will correspond to a false vacuum bubble in the Jordan frame.

We obtained the bounce solution in Figure 11. Here, we denote Φ, ρ, and $\dot{\rho}$. Therefore, we confirmed that a false vacuum bubble is possible even in the $\omega > -3/2$ cases.

4 Nucleation and evolution of vacuum bubbles in the thin wall approximation

In this section, we calculate the probability of bounces in the thin wall approximation. In the thin wall approximation, we assume that the transition region is sufficiently thin. Then

$$\dot{\Phi} \frac{\dot{\rho}}{\rho} \ll 1, \tag{37}$$

since $\dot{\Phi} \sim 0$ for the inside and the outside of the wall and $\bar{\rho}$ is sufficiently large on the wall.

We can then approximate the Einstein equation by

$$G_{\eta\eta} = 3\frac{\dot{\rho}^2 - 1}{\rho^2} = -3\frac{\dot{\rho}}{\rho}\frac{\dot{\Phi}}{\Phi} + \frac{\omega}{2}\left(\frac{\dot{\Phi}}{\Phi}\right)^2 - \frac{V}{2\Phi} \tag{38}$$

$$\simeq \frac{\omega}{2}\left(\frac{\dot{\Phi}}{\Phi}\right)^2 - \frac{V}{2\Phi}. \tag{39}$$

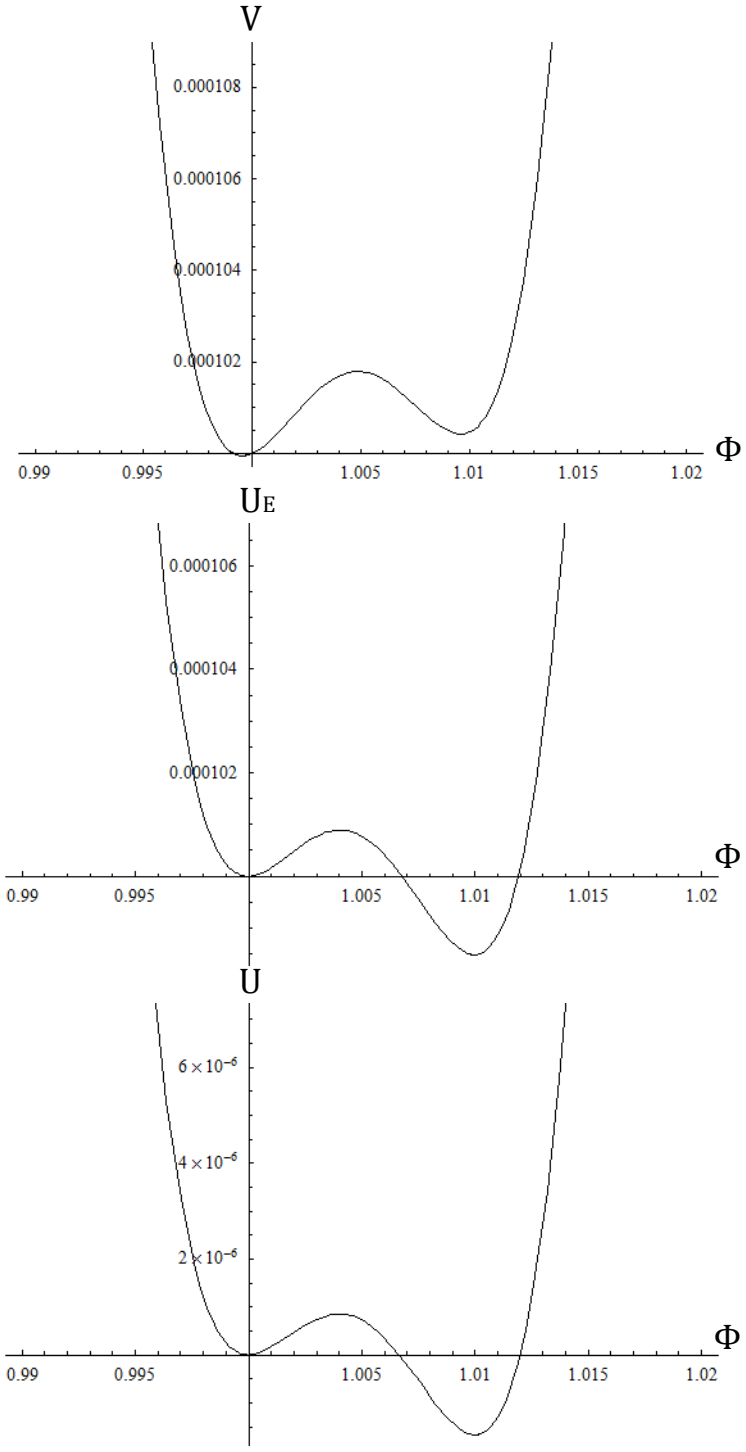

Figure 10: For $\omega = 10$, $A = 10^4$, $\Phi_{\rm f} - \Phi_{\rm t} = 0.01$, $\delta = -0.001$, and $V_0 = 0.0001$, we plot potentials V, U_E, and U.

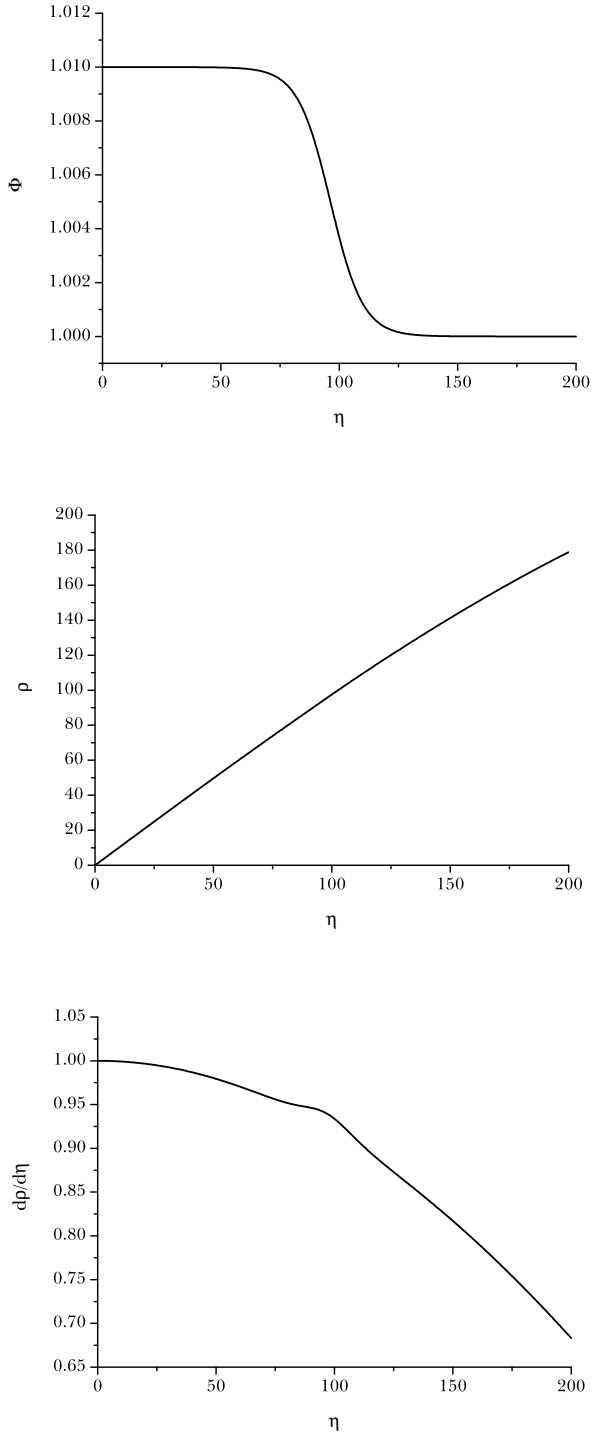

Figure 11: For $\omega = 10$, $A = 10^4$, $\Phi_{\rm f} - \Phi_{\rm t} = 0.01$, $\delta = -0.001$, and $V_0 = 0.0001$, we obtained a false vacuum bubble solution. We plot Φ, ρ, and $\dot{\rho}$ as functions of η.

Then we approximate $\dot{\rho}$ by

$$\dot{\rho}^2 = 1 - \rho\dot{\rho}\frac{\dot{\Phi}}{\Phi} + \frac{\rho^2}{6\Phi^2}\left(\omega\dot{\Phi}^2 - \Phi V\right) \tag{40}$$

$$\simeq 1 + \frac{\rho^2}{6\Phi^2}\left(\omega\dot{\Phi}^2 - \Phi V\right), \tag{41}$$

and obtain

$$\frac{d\rho}{d\eta} = \sqrt{1 + \frac{\rho^2}{6\Phi^2}\left(\omega\dot{\Phi}^2 - \Phi V\right)}. \tag{42}$$

Therefore, in the inside and the outside of the wall, we obtain

$$\frac{d\rho}{d\eta} = \sqrt{1 - \frac{\rho^2}{6\Phi}V}. \tag{43}$$

Also, we can obtain the following from the field equation by the thin wall approximation:

$$\dot{\Phi}\ddot{\Phi} = \frac{1}{2}\frac{d\dot{\Phi}^2}{d\eta} \tag{44}$$

$$\simeq \left(\frac{1}{2\omega+3}\left(\Phi V'(\Phi) - 2V(\Phi)\right)\right)\frac{d\Phi}{d\eta} \tag{45}$$

and obtain

$$\frac{d\Phi}{d\eta} = \sqrt{\frac{2}{2\omega+3}}\sqrt{\int_{\Phi_{\rm i}}^{\Phi}\left(\bar{\Phi}V'(\bar{\Phi}) - 2V(\bar{\Phi})\right)d\bar{\Phi}} \tag{46}$$

$$= \sqrt{\frac{2}{2\omega+3}}\sqrt{U(\Phi) - U(\Phi_{\rm i})}, \tag{47}$$

where $\Phi_{\rm i}$ is the field value of the inside of the bubble. Then, if $U(\Phi_{\rm i}) < U(\Phi)$ and we consider a true vacuum bubble in a false vacuum background, $2\omega+3$ should be positive; if $U(\Phi_{\rm i}) > U(\Phi)$ and we consider a false vacuum bubble in a true vacuum background, $2\omega+3$ should be negative. In our previous bounce examples, these correlations hold for all cases.

The probability is then

$$P \sim Ae^{-B}, \tag{48}$$

where

$$B = B_{\rm outside} + B_{\rm wall} + B_{\rm inside} \tag{49}$$

and

$$B_{\rm outside} = S_{\rm E}({\rm bounce}|\rho > \bar{\rho}) - S_{\rm E}({\rm background}|\rho > \bar{\rho}), \tag{50}$$

$$B_{\rm wall} = S_{\rm E}({\rm bounce}|\rho = \bar{\rho}) - S_{\rm E}({\rm background}|\rho = \bar{\rho}), \tag{51}$$

$$B_{\rm inside} = S_{\rm E}({\rm bounce}|\rho < \bar{\rho}) - S_{\rm E}({\rm background}|\rho < \bar{\rho}). \tag{52}$$

Here, $S_{\rm E}(\cdots|\rho > \bar{\rho})$, $S_{\rm E}(\cdots|\rho = \bar{\rho})$, and $S_{\rm E}(\cdots|\rho < \bar{\rho})$ mean integrations of the Lagrangian density of the solution (bounce or background) for $\rho > \bar{\rho}$, $\rho = \bar{\rho}$, and $\rho < \bar{\rho}$, respectively.

4.1 True vacuum bubbles in a false vacuum background

For a true vacuum bubble in a false vacuum background, we purpose the following field combination:

$$\Phi(\eta) = \begin{cases} \Phi_{\rm f} & \rho(\eta) > \bar{\rho}, \\ 1 & \rho(\eta) < \bar{\rho}, \end{cases} \tag{53}$$

where $\bar{\rho}$ is the location of the wall and the transition region is sufficiently thin. Here, we assume that

$$V(\Phi) = \begin{cases} V_0 & \Phi = 1, \\ \Lambda & \Phi = \Phi_{\rm f}. \end{cases} \tag{54}$$

We then obtain the following quantities (using Equations (43) and (47)):

$$B_{\rm outside} = 0 \tag{55}$$

$$\begin{aligned} B_{\rm wall} &= \frac{\pi}{4}\int d\eta \left(\bar{\rho}^3 V(\Phi) - 6\bar{\rho}\Phi - \bar{\rho}^3\Lambda + 6\bar{\rho}\Phi_{\rm f}\right) && (56)\\ &= \frac{\pi}{4}\sqrt{\left|\frac{2\omega+3}{2}\right|}\int_1^{\Phi_{\rm f}} \frac{d\Phi}{\sqrt{|U(\Phi)-U(1)|}}\left(\bar{\rho}^3 V(\Phi) - 6\bar{\rho}\Phi - \bar{\rho}^3\Lambda + 6\bar{\rho}\Phi_{\rm f}\right) && (57)\\ &\equiv 2\pi^2\bar{\rho}^3\sigma(\omega,\bar{\rho}), && (58) \end{aligned}$$

$$\begin{aligned} B_{\rm inside} &= \frac{\pi}{4}\int d\eta \left(\rho^3 V_0 - 6\rho - \rho^3\Lambda + 6\rho\Phi_{\rm f}\right) && (59)\\ &= \frac{3\pi}{2}\left[-\frac{2}{V_0}\left(1-\left(1-\frac{V_0}{6}\bar{\rho}^2\right)^{3/2}\right) + \frac{2\Phi_{\rm f}^2}{\Lambda}\left(1-\left(1-\frac{\Lambda}{6\Phi_{\rm f}}\bar{\rho}^2\right)^{3/2}\right)\right]. && (60) \end{aligned}$$

Here, we define the tension function of the thin wall $\sigma \equiv B_{\rm wall}/2\pi^2\bar{\rho}^3$ which is a function of ω and $\bar{\rho}$.

As an example, in Figure 12, we plot the function B for $\omega = 10$, $A = 10^4$, $\delta = 0.0025$, $\Phi_{\rm f} - \Phi_{\rm t} = 0.025$, and $V_0 = 0$ case. This figure shows that there is a stationary point that indicates the size of the bubble and probability.

4.2 False vacuum bubbles in a true vacuum background

We purpose the following field combination

$$\Phi(\eta) = \begin{cases} 1 & \rho(\eta) > \bar{\rho}, \\ \Phi_{\rm f} & \rho(\eta) < \bar{\rho}, \end{cases} \tag{61}$$

where $\bar{\rho}$ is the location of the wall and the transition region is sufficiently thin. Here, we assume that

$$V(\Phi) = \begin{cases} V_0 & \Phi = 1, \\ \Lambda & \Phi = \Phi_{\rm f}. \end{cases} \tag{62}$$

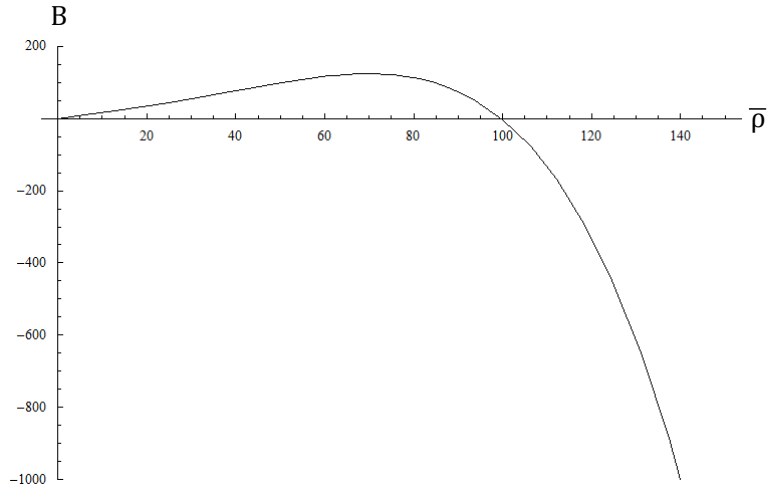

Figure 12: $B(\bar{\rho})$ for a true vacuum bubble in a false vacuum background: $\omega = 10$, $A = 10^4$, $\delta = 0.0025$, $\Phi_{\rm f} - \Phi_{\rm t} = 0.025$, and $V_0 = 0$.

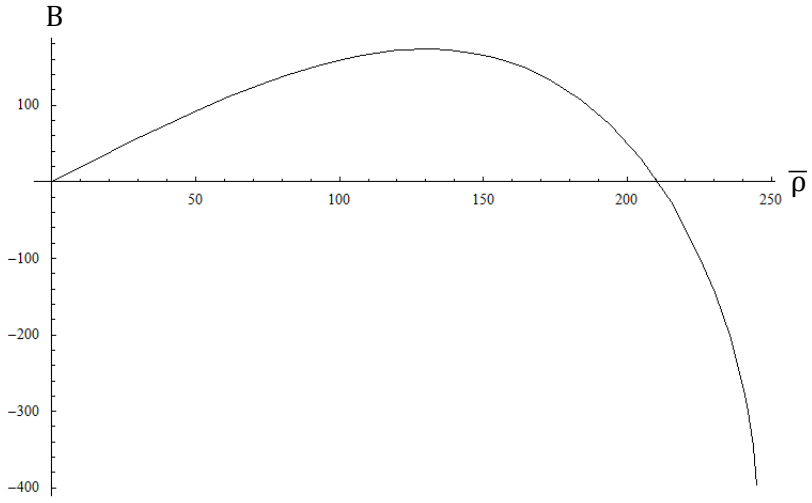

Figure 13: $B(\bar{\rho})$ for a false vacuum bubble in a true vacuum background: $\omega = 10$, $A = 10^4$, $\Phi_{\rm f} - \Phi_{\rm t} = 0.01$, $\delta = -0.001$, and $V_0 = 0.0001$. Then $V(T) < V(F)$ and $U_E(T) > U_E(F)$.

Then, as in the previous subsection, we obtain the following quantities (using Equations (43) and (47)):

$$B_{\rm outside} = 0, \tag{63}$$

$$\begin{aligned} B_{\rm wall} &= \frac{\pi}{4}\int d\eta \left(\bar{\rho}^3 V(\Phi) - 6\bar{\rho}\Phi - \bar{\rho}^3 V_0 + 6\bar{\rho}\right) && (64)\\ &= \frac{\pi}{4}\sqrt{\left|\frac{2\omega+3}{2}\right|}\int_{\Phi_{\rm f}}^{1} \frac{d\Phi}{\sqrt{|U(\Phi)-U(\Phi_{\rm f})|}}\left(\bar{\rho}^3 V(\Phi) - 6\bar{\rho}\Phi - \bar{\rho}^3 V_0 + 6\bar{\rho}\right) && (65)\\ &\equiv 2\pi^2\bar{\rho}^3\sigma(\omega,\bar{\rho}), && (66) \end{aligned}$$

$$\begin{aligned} B_{\rm inside} &= \frac{\pi}{4}\int d\eta \left(\rho^3\Lambda - 6\rho\Phi_{\rm f} - \rho^3 V_0 + 6\rho\right) && (67)\\ &= \frac{3\pi}{2}\left[-\frac{2\Phi_{\rm f}^2}{\Lambda}\left(1-\left(1-\frac{\Lambda}{6\Phi_{\rm f}}\bar{\rho}^2\right)^{3/2}\right) + \frac{2}{V_0}\left(1-\left(1-\frac{V_0}{6}\bar{\rho}^2\right)^{3/2}\right)\right]. && (68) \end{aligned}$$

As an example, in Figure 13, we plot the function B for the $\omega = 10$, $A = 10^4$, $\Phi_{\rm f} - \Phi_{\rm t} = 0.01$, $\delta = -0.001$, and $V_0 = 0.0001$ case. This figure shows that there is a stationary point that indicates the size of the bubble and probability.

4.3 Dynamics of vacuum bubbles in the Lorentzian signatures

Let us assume that a thin wall bubble has a field value Φ_- for inside and Φ_+ for outside. The junction equation then takes the following form [17]:

$$\epsilon_-\Phi_-\sqrt{\dot{\bar{\rho}}^2 + f_-} - \epsilon_+\Phi_+\sqrt{\dot{\bar{\rho}}^2 + f_+} = 4\pi\bar{\rho}\sigma_0, \tag{69}$$

where

$$f_\pm = 1 - \frac{V(\Phi_\pm)}{6\Phi_\pm}\bar{\rho}^2 \tag{70}$$

and $\epsilon_\pm$ are $+1$ if the outward normal to the wall is pointing towards increasing $\bar{\rho}$ and -1 if towards decreasing $\bar{\rho}$.

Note that the true vacuum bubble case and the false vacuum case can be transformed by $- \leftrightarrows +$ of each subscript and change $\sigma \to -\sigma$. Then, it is equivalent to change $\epsilon_\pm \to -\epsilon_\pm$ and flip $- \leftrightarrows +$ of each subscript. However, to obtain the potential $V_{\rm eff}(\bar{\rho})$ which holds

$$\frac{1}{2}\dot{\bar{\rho}}^2 + V_{\rm eff}(\bar{\rho}) = 0, \tag{71}$$

we do not need the information of the signs of each root. Therefore, the analysis of effective potentials is the same for both cases.

The authors studied the effective potential $V_{\rm eff}$ in [17] for false vacuum bubbles. It was found that there are two effective potentials $V_{\rm eff}^{(1,2)}(\bar{\rho})$, and it is not difficult to confirm that each effective

	$\Phi_+ > 1$	$\Phi_+ < 1$
$\epsilon_+^{(1)}$	$\pm$	$\pm$
$\epsilon_-^{(1)}$	$+$	$+$
$\epsilon_+^{(2)}$	$-$	$+$
$\epsilon_-^{(2)}$	$-$	$+$

Table 3: Summary of the signs for true vacuum bubbles. $\pm$ depends on tensions.

	$\Phi_- > 1$	$\Phi_- < 1$
$\epsilon_+^{(1)}$	$-$	$-$
$\epsilon_-^{(1)}$	$\mp$	$\mp$
$\epsilon_+^{(2)}$	$+$	$-$
$\epsilon_-^{(2)}$	$+$	$-$

Table 4: Summary of the signs for false vacuum bubbles. $\mp$ depends on tensions.

potential is a monotonously decreasing function. Therefore, the causal structures are determined by $\epsilon_\pm$ in $\bar{\rho} \to \infty$ limit. The sign structures for $\epsilon_\pm$ are given in Tables 3 and 4. (We used the results in [17] to obtain Table 4, and we flipped the signs to obtain Table 3: $\epsilon_\pm \to -\epsilon_\pm$ and flip $- \leftrightarrows +$.) Also, the contents of each root never become zero; this implies that the asymptotic $\epsilon_\pm$ is always correct for our cases.

If we vary $B = B_{\rm outside} + B_{\rm wall} + B_{\rm inside}$ by $\bar{\rho}$ for both true and false vacuum bubble cases, we obtain

$$0 = \frac{\partial B}{\partial \bar{\rho}} = 6\pi^2 \bar{\rho}^2 \sigma(\omega, \bar{\rho}) + 2\pi^2 \bar{\rho}^3 \frac{\partial \sigma(\omega, \bar{\rho})}{\partial \bar{\rho}} + \frac{3\pi}{2} \bar{\rho} \left(-\Phi_- \sqrt{f_-} + \Phi_+ \sqrt{f_+} \right) \tag{72}$$

$$= \frac{3\pi}{2} \bar{\rho} \left(4\pi \bar{\rho} \left(\frac{\bar{\rho}}{3} \frac{\partial \sigma}{\partial \bar{\rho}} + \sigma \right) - \Phi_- \sqrt{f_-} + \Phi_+ \sqrt{f_+} \right) \tag{73}$$

If we define $\sigma_0 \equiv \frac{\bar{\rho}}{3} \frac{\partial \sigma}{\partial \bar{\rho}} + \sigma$, we derive the solution of Equation (69) and $\epsilon_\pm = +1$. This smoothly joins the Euclidean patch to the Lorentzian patch at the $t = 0$ surface.

Here, $\epsilon_\pm = +1$ imply that for true vacuum bubbles, we use $V_{\rm eff}^{(1)}$ or $V_{\rm eff}^{(2)}$ with $\Phi_+ < 1$; $\Phi_+ > 1$ and $V_{\rm eff}^{(2)}$ is disallowed. However, for false vacuum bubbles, only $\Phi_- > 1$ and $V_{\rm eff}^{(2)}$ is allowed. For each allowed case, $\epsilon_\pm = +1$ imply that each bubbles expand over background. For the false vacuum case, the result is consistent with our previous paper [17]: the only expanding bubble in a nearly flat background is only for $\Phi_- > 1$ and $V_{\rm eff}^{(2)}$ case.

In all cases, if the solution is allowed, $\epsilon_\pm = +1$ implies that each bubble can expand over the background. For a false vacuum bubble case, $\Phi_- > 1$ is not allowed and may imply that such

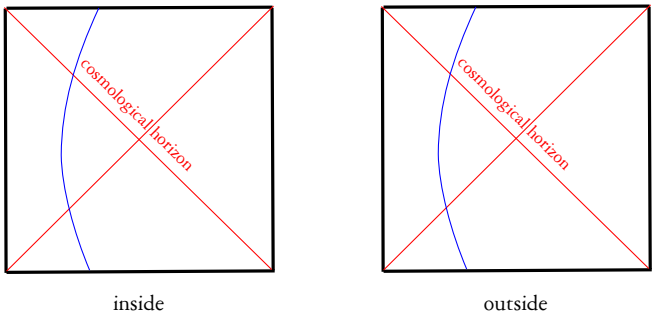

Figure 14: Causal structures for dS − dS cases. For a true vacuum bubble, the inside cosmological horizon is larger than the outside cosmological horizon; for a false vacuum bubble, the inside cosmological horizon is smaller than the outside cosmological horizon.

a bubble is unstable even though it is nucleated. For allowed false vacuum solutions, the causal structure of the wall will be Figure 14. For a false vacuum bubble, there is a time where a false vacuum bubble is larger than the inside cosmological horizon while it is smaller than the outside cosmological horizon. In this case, if one sends a pulse of energy to the bubble and induces an apparent horizon, and if the apparent horizon is larger than the size of the bubble, a de Sitter black hole can be seen that separates the inside bubble universe and the outside.

5 Discussion

In this paper, we study nucleation of vacuum bubbles in the Brans-Dicke type theory of gravity. In the Euclidean signatures, we first calculate field combinations of vacuum bubbles as solutions of Einstein and field equations. Second, we calculate the probabilities by integrating the Euclidean action assuming the thin wall approximation.

The Einstein equation is determined by the potential of the Brans-Dicke field while the dynamics of the Brans-Dicke field is determined by the effective potential, which can be distinct from the original potential. We illustrate three possible ways to obtain vacuum bubbles: true vacuum bubbles for $\omega > -3/2$, false vacuum bubbles for $\omega < -3/2$, and false vacuum bubbles for $\omega > -3/2$ when the vacuum energy of the false vacuum in the potential of the Einstein frame is *less* than that of the true vacuum. After the bubble is nucleated at the $t = 0$ surface, we can smoothly connect and match the field combinations to some solutions of the Lorentzian signatures and consistently continue their subsequent evolutions.

One note of caution should be made regarding the conformal transformation between the Jordan frame and the Einstein frame. For true vacuum bubbles with $\omega > -3/2$, the nucleation of the

bubble is not strange, since Einstein gravity also allow such possibility. For false vacuum bubbles with $\omega < -3/2$, the nucleation of the bubble is also not strange since $\omega < -3/2$ means that the conformal transformation is not well-defined or the defined scalar field in the Einstein frame behaves as a ghost. However, if a false vacuum bubble in $\omega > -3/2$ is possible, it will eventually expand and inflate, and there should then be a region on the wall where the null energy condition is violated. In the Jordan frame, this is not a problem [18]; however, in the Einstein frame with $\omega > -3/2$, it appears to be a problem. In this paper, our solution does not suffer this paradoxical situation, since a false vacuum bubble in the Jordan frame corresponds to a true vacuum bubble in the Einstein frame. Then, in the Einstein frame, there is no reason to conclude that such a bubble violates the null energy condition. Also, it is not so strange although we obtain a small false vacuum bubble, since a nucleation of a true vacuum bubble in the Einstein frame is generally possible.

Then, two interesting questions are raised. First, can we describe the conformal transformation on the wall? Second, which frame is physical? If the Einstein frame is physical, no discussions on false vacuum bubbles will be meaningful. However, if the Jordan frame can be physical, the generation of a false vacuum bubble is an allowed event. It is known that there is controversy regarding the latter question [8] and the most conservative interpretation is that two frames are equivalent, at least in the classical level. If we include quantum effects in a fixed frame, then the frame will be chosen to be physical. In this sense, the choice of the Jordan frame is still a viable option. We leave the two questions as future work.

We conclude that, in general scalar-tensor theories or Brans-Dicke type theories, which can include some models of string theory, vacuum bubbles are allowed; not only true vacuum bubbles but also false vacuum bubbles. One potential problem is that, if we wish to derive a scalar-tensor or Brans-Dicke type model from string theory, the model may be related to dilaton gravity; but in dilaton gravity, the potential of the dilaton field is restricted by the theory. If we assume a special condition on the potential, then dilaton gravity can generate a false vacuum bubble; however, it is necessary to assess whether dilaton gravity can allow such a special potential. We also leave this as future work.

Acknowledgments

DY would like to thank Ewan Stewart for discussions and encouragement. DY and YJL were supported by Korea Research Foundation grants (KRF-313-2007-C00164, KRF-341-2007-C00010) funded by the Korean government (MOEHRD) and BK21. BHL and WL were supported by a Korea Science and Engineering Foundation (KOSEF) grant funded by the Korean government (MEST)

through the Center for Quantum Spacetime (CQUeST) of Sogang University with grant number R11 - 2005 - 021. WL was supported by the National Research Foundation of Korea Grant funded by the Korean Government (Ministry of Education, Science and Technology)[NRF-2010-355-C00017].

References

[1] C. Brans and C. H. Dicke, Phys. Rev. **124**, 925 (1961).

[2] C. M. Will, *"Was Einstein Right?,"* New York, Basic Books (1986).

[3] S. Weinberg, *"Gravitation and Cosmology,"* John Wiley and Sons (1972).

[4] H. Kim, Phys. Lett. B **606**, 223 (2005);
H. Kim, Mon. Not. Roy. Astron. Soc. **364**, 813 (2005).

[5] M. B. Voloshin, I. Yu. Kobzarev, and L. B. Okun, Yad. Fiz. **20**, 1229 (1974) [Sov. J. Nucl. Phys. **20**, 644 (1975)];
S. R. Coleman, Phys. Rev. D **15**, 2929 (1977) [Erratum-ibid. Phys. Rev. D **16**, 1248 (1977)];
C. G. Callan and S. R. Coleman, Phys. Rev. D **16**, 1762 (1977).

[6] S. R. Coleman and F. De Luccia, Phys. Rev. D **21**, 3305 (1980).

[7] W. Lee, B. H. Lee, C. H. Lee and C. Park, Phys. Rev. D **74**, 123520 (2006) [arXiv:hep-th/0604064];
W. Lee, C. Park, B.-H. Lee, and C. H. Lee, J. Korean Phys. Soc. **50**, S85 (2007);
B. H. Lee, C. H. Lee, W. Lee, S. Nam and C. Park, Phys. Rev. D **77**, 063502 (2008) [arXiv:0710.4599 [hep-th]];
B. H. Lee, C. H. Lee, W. Lee, S. Nam and C. Park, J. Korean Phys. Soc. **53**, 1101 (2008).

[8] V. Faraoni, *"Cosmology in scalar tensor gravity,"* Kluwer Academic Publishers (2004).

[9] B. Bertotti, L. Iess and P. Tortora, Nature **425**, 374 (2003).

[10] M. Gasperini, *"Elements of string cosmology,"* Cambridge, Cambridge University Press (2007).

[11] S. Foffa, M. Maggiore and R. Sturani, Nucl. Phys. B **552**, 395 (1999) [arXiv:hep-th/9903008].

[12] L. Randall and R. Sundrum, Phys. Rev. Lett. **83**, 3370 (1999) [arXiv:hep-ph/9905221].

[13] J. Garriga and T. Tanaka, Phys. Rev. Lett. **84**, 2778 (2000) [arXiv:hep-th/9911055].

[14] Y. Fujii and K. Maeda, *"The scalar-tensor theory of gravitation,"* Cambridge, Cambridge University Press (2003).

[15] K. M. Lee and E. J. Weinberg, Phys. Rev. D **36**, 1088 (1987).

[16] B.-H. Lee and W. Lee, Classical Quantum Gravity **26**, 225002 (2009) [arXiv:0809.4907].

[17] B. H. Lee, W. Lee and D. Yeom, arXiv:1006.3127 [gr-qc].

[18] G. Kang, Phys. Rev. D **54**, 7483 (1996) [arXiv:gr-qc/9606020];
D. Hwang and D. Yeom, Class. Quant. Grav. **27**, 205002 (2010) [arXiv:1002.4246 [gr-qc]].